Tellus SERIES A DYNAMIC METEOROLOGY AND OCEANOGRAPHY
PUBLISHED BY THE INTERNATIONAL METEOROLOGICAL INSTITUTE IN STOCKHOLM

Atmospheric energy transport to the Arctic 1979–2012

By SONG-MIAO FAN*, LUCAS M. HARRIS and LARRY W. HOROWITZ,
NOAA Geophysics Fluid Dynamics Laboratory, Princeton, New Jersey, USA

(Manuscript received 17 June 2014; in final form 16 October 2015)

ABSTRACT

The Arctic troposphere has warmed faster than the global average over the last several decades. It was suggested that atmospheric northward energy transport (ANET) into the Arctic had contributed to tropospheric warming in the Arctic. Here we calculate ANET based on the NCEP/NCAR reanalysis data from 1979 to 2012. During this period the zonally integrated energy flux into the Arctic has decreased rather than increased in all seasons. However, the trends are statistically insignificant except for the winter and annual mean fluxes. For the winter season, the transient eddy flux of energy increases over Greenland and the Greenland Sea and decreases over west-central Siberia (WCS). Trends in meridional wind variance and vorticity also indicate increasing transient eddy activity over Northern Canada, the Greenland Sea and the Norwegian Sea and decreasing activity over WCS. Inter-winter variations in local vorticity over the WCS are significantly anti-correlated with the Arctic climate.

Keywords: climate dynamics, Arctic climate warming amplification

1. Introduction

Arctic amplification (AA) of global warming has been observed in both the upper and lower troposphere in the last few decades (e.g., Graversen et al., 2008; Alexeev et al., 2012; Screen et al., 2012). Chung et al. (2013) evaluated the warming in the Arctic using four different reanalysis data sets and radio-soundings for the period 1979–2011. Significant warming trends are found for all seasons in all data sets, and two times greater rates of warming are found in the lower troposphere than in the upper troposphere. The annual mean surface temperature poleward of 70°N increased by a range of 1.75 ± 0.29 K to 2.71 ± 0.28 K over 33 years, 4–6 times larger than the global average surface air temperature increase (Arguez et al., 2013), and the warming in winter months (December–January–February, hereafter DJF) was about twice as large as in summer months (June–July–August). With four-times present CO_2 in the atmosphere, contemporary global climate models predict a surface warming of 4.3 K in the tropics (30°S–30°N) and 11.2 K in the Arctic (60°N–90°N), with a range of 3–6 K and 5–16 K, respectively (Pithan and Mauritsen, 2014). AA of climate change has been observed in geological records and is now recognised as an inherent characteristic of the global climate system (Serreze and Barry, 2011). Multiple feedback effects can contribute to AA, including albedo, lapse rate and water vapour (Cai, 2005; Winton, 2006; Taylor et al., 2013; Graversen et al., 2014; Pithan and Mauritsen, 2014). Additional warming may result from changes in arctic vegetation (Swann et al., 2010) and black carbon in snow (Flanner et al., 2007).

The arctic warming over the past decade has been accompanied by a rapid decline in sea ice concentrations in the polar region (Comiso et al., 2008; Comiso, 2012). Changes in sea ice extent impact heat fluxes between the ocean and the atmosphere (Smedrud et al., 2013), and may have contributed to the Arctic surface warming (Serreze et al., 2009; Screen and Simmonds, 2010). In model simulations, local sea ice and sea surface temperature (SST) trends explain a large portion of the observed Arctic near-surface warming, whereas remote SST changes explain the majority of observed warming aloft (Screen et al., 2012). Over longer time scales, the multidecadal oscillation of the Atlantic meridional overturning circulation (AMOC) may modulate Arctic sea ice and surface air temperature (SAT) (Chylek et al., 2009; Mahajan et al., 2011; Peings and Magnusdottir, 2014).

The vertical structure of the recent arctic warming as represented in observed data and reanalysis products has gained much deserved attention (Graversen et al., 2008; Alexeev et al., 2012; Screen et al., 2012; Chung et al., 2013). The warming aloft is not attributable to shortwave and longwave (LW) feedbacks, nor to changes in sea ice and SST

*Corresponding author.
email: Songmiao.Fan@noaa.gov

Citation: Tellus A 2015, **67**, 25482, http://dx.doi.org/10.3402/tellusa.v67.25482

within the Arctic. Graversen et al. (2008) proposed atmospheric northward energy transport (ANET) as an important mechanism for the recent arctic warming. Mid-tropospheric temperatures in the Arctic are sensitive to advection of energy into the Arctic: the 500 hPa temperature field in the Arctic was found to be positively correlated with ANET across 60°N with a lag of 5 days (Graversen et al., 2008). The correlation may be robust on the synoptic time scale, but, on longer time scales, a reduced zonal-mean meridional temperature gradient may cause a decrease of energy transport (Serreze and Barry, 2005).

Other studies have searched for changes in large-scale atmospheric circulation patterns as potential causes. Remote SST patterns might affect arctic meteorological conditions through teleconnections (Screen et al., 2012; Perlwitz et al., 2015). However, details of the dynamical processes are not known to date. In a recent study based on the ERA-Interim reanalysis product, Woods et al. (2013) found that the interannual variability of intense moisture intrusions across 70°N is strongly correlated with variability in winter-mean surface downward LW radiation and skin temperature averaged over the Arctic. The intense intrusions are caused by large-scale blocking patterns which deflect mid-latitude cyclones and their associated moisture poleward. The above studies thus emphasise the importance of understanding the variability in large-scale circulation and its impacts on energy transport into the Arctic, the surface energy budget and top-of-atmosphere (TOA) net radiative flux.

In this study, we first extend the analysis of Graversen et al. (2008) based on ERA-40 reanalysis data to NCEP/NCAR reanalysis data. We examine energy transport by planetary and transient waves through height–longitude cross-sections and by the zonal mean circulation (ZMC). Section 2 describes the data and methods. Section 3 presents the energy fluxes and trends. Section 4 discusses inter-annual variations in winter. Section 5 summarises the results and conclusions.

2. Data and analysis method

The total energy per unit mass of air is given by $E = c_v T + gz + Lq + \frac{1}{2}(u^2 + v^2)$, where c_v is heat capacity, T is temperature, g is gravity, z is geopotential height, L is latent heat, q is specific humidity, u is zonal wind and v is meridional wind. The energy balance in a polar cap is given by Peixoto and Oort (1992) (Eq. 13.38 with the over bars for time averaging neglected):

$$\frac{\partial}{\partial t}\int (c_v T + gz + Lq)\,dm = \iint_{\text{wall}} (c_p T + gz + Lq)\,v\,\frac{dx\,dp}{g} + F_{TA} - F_{BA}$$

where m is mass, c_p is heat capacity at constant pressure, v is meridional wind, x is zonal distance, p is pressure ($p = p_s\sigma$ at a sigma-level, p_s = surface pressure), F_{TA} and F_{TB} are downward energy fluxes at top and bottom of the atmosphere, respectively.

We calculate mass-weighted surface-TOA and surface-400 hPa northward fluxes of internal energy (denoted by vT), potential energy (vz) and latent heat (vq) using the NCEP/NCAR reanalysis data from 1979 to 2012 (Kalnay et al., 1996). The reanalysis data is archived at 6-hourly intervals, 28 vertical sigma-levels, 192 longitude bands and 94 latitude bands. The kinetic energy flux is small and is neglected. We decompose the fluxes into contributions by stationary waves (denoted by v*q*, v*T* and v*z*) and transient eddies (v'q', v'T' and v'z') and by the monthly ZMC ([v][q], [v][T] and [v][z]) (Peixoto and Oort, 1992). We define transient eddies as departures from monthly mean quantities in each grid, and stationary waves as departures from zonal mean averages for each vertical level and in each month. Vertically averaged zonal mean v is subtracted from the mean v in each layer to ensure a zero net mass flux through a "wall" encircling the Arctic and to eliminate spurious results (Trenberth, 1991; Graversen, 2006). We also calculate monthly, mass-weighted variances of meridional wind (v'v'), mean positive relative vorticity (*vort*) and the time fraction for which $vort > 1.0 \times 10^{-5}\ s^{-1}$ as measures of cyclone activity (Sorteberg and Walsh, 2008). Analyses are performed for twelve 30°-wide longitudinal sectors (Fig. 1). The time series for each cross-section are analysed for interannual variability and linear trends from 1979 to 2012. Unless otherwise noted all analyses are performed for northern winter (DJF).

3. Energy fluxes by transient eddy and trends

In this section, we present an analysis of poleward energy fluxes. Figure 2 shows the ANET fluxes at 65.7°N and 71.4°N, which are divided by the encircled surface areas. The monthly mean fluxes (Fig. 2a) at 71.4°N are in good agreement with a previous calculation at 70°N based on a 10-year data set (Nakamura and Oort, 1988, as tabulated in Serreze and Barry, 2005). The annual cycle of ANET shows a broad peak from November to March and a minimum from May to July/August. The annual and seasonal mean ANET show large interannual variations and downward trends (Fig. 2b–f). The linear trends from 1979 to 2012 are shown in Table 1 for ANET at 65.7°N. The annual and winter trends are significant at 2 standard deviations (s.d.), while the trends in other seasons are insignificant. In comparison, calculations of ANET based on ERA-40 reanalysis data for 1979–2001 show a downward trend in winter and an upward trend in summer (Graversen, 2006; Graversen et al., 2008). The trend in ANET at 60°N explains only a fraction (e.g., 20–30% near 700 hPa) of the temperature trends in summer (Graversen et al., 2008).

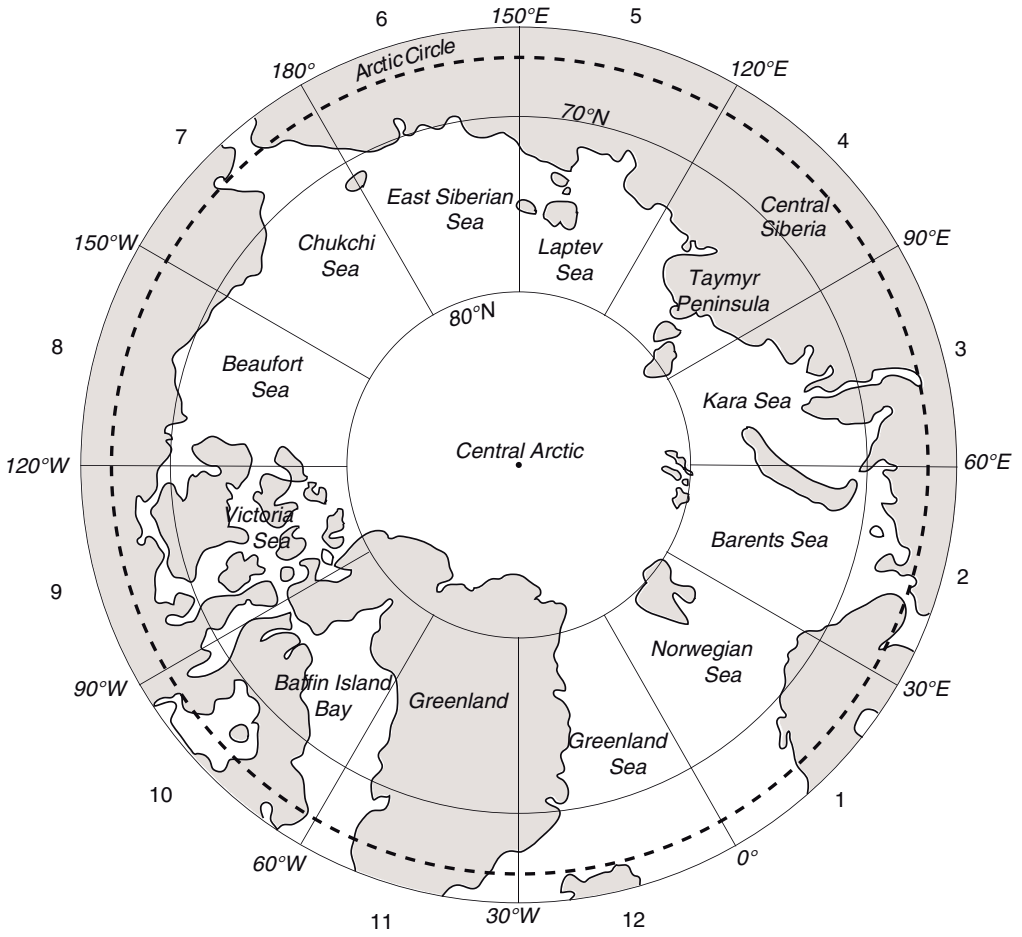

Fig. 1. Longitude sections used in this study (adapted from Sorteberg and Walsh, 2008). Each section is referred to by a number (1–12) and its adjacent ocean or land region. The dashed line indicates the Arctic Circle (66.6°N).

A partitioning of the ANET in winter is shown in Table 2. Transport of sensible heat is much larger than latent heat and together they tend to warm the Arctic. Transport of geopotential energy is dominated by the ZMC which tends to cool the Arctic. Transport by stationary waves is comparable to that by transient eddies. The total flux at 65.7°N (2516 TW) is larger than that at 71.4°N (1545 TW) due to a net radiative cooling in between the latitudes.

Figure 3 shows the averages and linear trends of the energy flux terms by transient eddies through the cross-sections from the surface to ~400 hPa in winters from 1979 to 2012, and the same for the variances of v and for the averages of positive vorticity. The effect of transient baroclinic waves on energy transport are most pronounced below 400 hPa. The largest energy fluxes occur over the Greenland Sea (GS) (Sector 12), the Norwegian Sea (NS) (Sector 1) and the Chukchi Sea (Sector 7), where the air is warmer and contains more water vapour than over land. The land–ocean contrast is more pronounced for latent heat (Fig. 3a) than sensible heat (Fig. 3c). The sensible heat fluxes are greater than the latent heat fluxes by more than a factor of 2. The lowest fluxes are estimated for cross-sections (4 and 5) over Central Siberia and the mountainous region to the east of 120°E where the air is extremely cold and dry under persistent high pressures. More transient eddy activity occurs over the North Atlantic than other regions as indicated by the variances of v (Fig. 3g) and the mean positive local vorticities (Fig. 3i), contributing to the land-ocean contrast in eddy fluxes of energy.

Consistent decreases from 1979 to 2012 in transient eddy activities and associated energy fluxes are shown for cross-sections 3 and 4 (60°–120°E) over regions south of the Kara Sea and Taymyr Peninsula in western and central Siberia (Figs. 1 and 3). Winter blocking frequency was found to have increased for the same time period over western and central Siberia as shown by the time-series of average frequency for 40°–80°N and 60°–120°E (Barnes et al., 2014). Less significant but apparent increases of northward energy fluxes are shown in Fig. 3b, d and f for cross-sections 10–12 (270°–360°E, Fig. 1) over the regions extending from the Baffin Islands/Bay to Greenland and the GS. Transient eddy

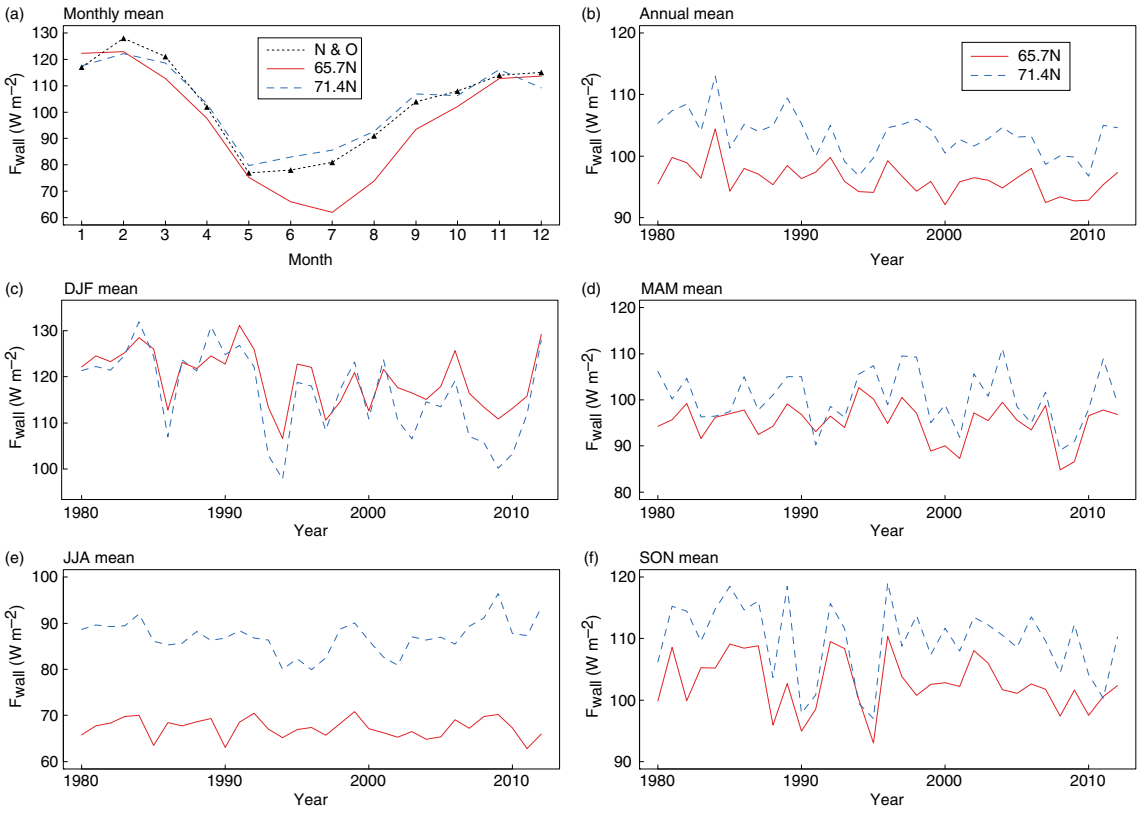

Fig. 2. Zonally and vertically integrated poleward heat transport (F_{wall}) calculated at 65.7°N and 71.4°N, respectively. The fluxes are normalised by the enclosed polar surface areas to facilitate inter-comparison with radiative fluxes. (a) Monthly mean fluxes for the period 1979–2012; N&O indicates 10-year average fluxes calculated at 70°N by Nakamura and Oort (1988). (b)–(f) Annual, DJF, MAM, JJA and SON mean fluxes.

activity appears to have become stronger over the NS and the GS (sections 1 and 12, Fig. 3h and j).

4. Interannual variability of transport in the North Atlantic and Siberia

In this section, we examine the interannual variability as well as the long-term trend in transient eddies in the northern Atlantic and Siberia. Figure 4 shows the winter mean positive vorticity and the time fraction of high vorticity (TFHV: $vort > 1.0 \times 10^{-5}$ s^{-1}) in the mid-troposphere (approximately 400–700 hPa) over the GS and the NS (30°W to 30°E) and over west-central Siberian (WCS) (60°E to 120°E), respectively. Over the GS and NS, the mean *vort* is generally above the long-term average during 2000–2012 and is lower during the earlier period (Fig. 4a). The TFHV

Table 1. Linear trends of atmospheric northward energy transport at 65.7°N (divided by the total area north of the latitude) between 1979 and 2012

	Trend ± s.d. (W m^{-2} a^{-1})
Annual	−0.13 ± 0.04
DJF	−0.26 ± 0.10
MAM	−0.07 ± 0.07
JJA	−0.03 ± 0.04
SON	−0.11 ± 0.08

Table 2. Partitioning of atmospheric northward energy transport (in terawatt) in winter (DJF) between 1979 and 2012

Flux terms	65.7°N	71.4°N
Stationary		
[v*q*]	90	20
[v*T*]	1205	285
[v*z*]	742	951
Transient		
[v'q']	240	128
[v'T']	1145	771
[v'z']	231	156
Mean circulation		
[v][q]	8	9
[v][T]	145	189
[v][z]	−1288	−964
Total	2516	1545

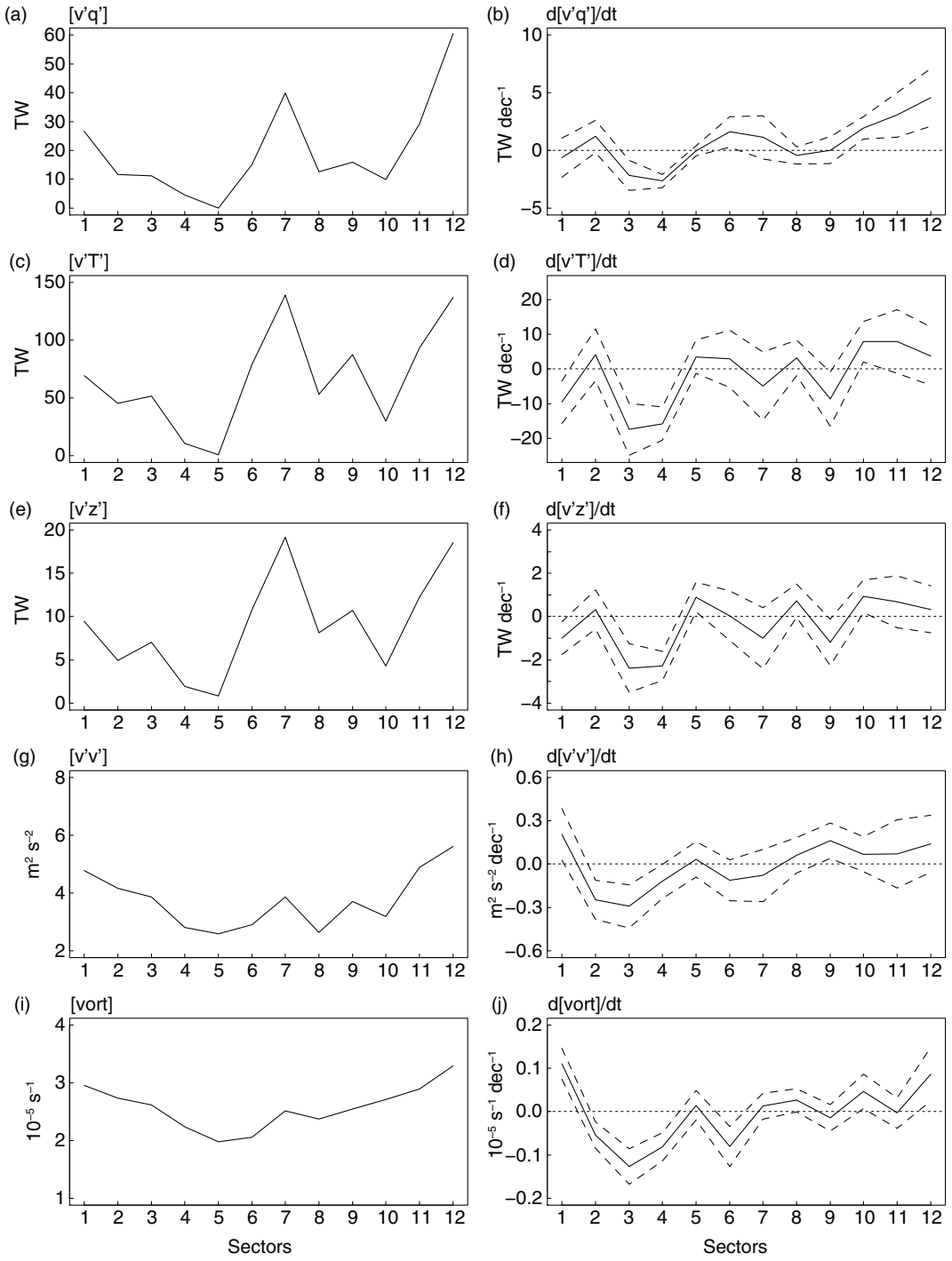

Fig. 3. Average wintertime (DJF) northward energy fluxes by transient eddies through cross-sections (~400 hPa – surface, 30° longitude bins) at 65.7°N near the Arctic Circle, variances of v-wind, positive vorticities and their respective linear trends between 1979 and 2012. Cross-section index increases eastward from 0° to 360°. Variances of v-wind and positive vorticities are calculated at 65.7°N and 71.4°N and averaged. (a) latent heat flux [v'q'], (b) d[v'q']/dt, (c) sensible heat flux [v'T'], (d) d[v'T']/dt, (e) potential energy flux [v'z'], (f) d[v'z']/dt, (g) v-wind variance [v'v'], (h) d/[v'v']/dt, (i) positive vorticity [*vort*], (j) d[*vort*]/dt. Dashed lines indicate ± 1-σ for the linear trends.

shows large year-to-year variations but no clear trend (Fig. 4c). Over the WCS, mean *vort* is often above the long-term average in the early years, close to average in the middle years and below average in the later years (Fig. 4b). The TFHV also shows a general decrease from 1980 to 2012 and large interannual variations (Fig. 4d).

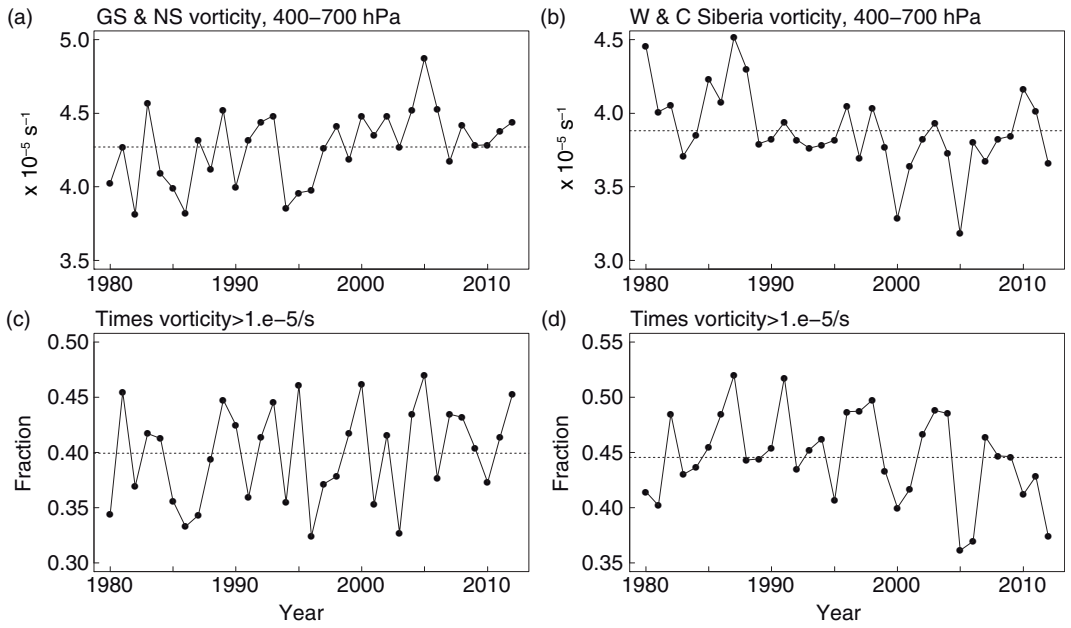

Fig. 4. Winter averages of high vorticity ($vort > 1.0 \times 10^{-5}\ s^{-1}$) between approximately 400 and 700 hPa at 65.7°N over the Greenland Sea (GS) to the Norwegian Sea (NS) (30°W–30°E) (a) and west-central Siberia (60°E–120°E) (b), and the time fraction of high local vorticity over the GS and NS (c) and W and C Siberia (d).

To demonstrate the impact of cyclone variability and trends shown in Fig. 4 on arctic climate, we calculate the winter mean precipitable water, skin temperature, upward TOA LW radiation and downward surface LW radiation north of 70°N, derived from NCEP reanalysis data (Fig. 5). These parameters show similar interannual variations and long-term trends with large correlation coefficients between each pair, except for the TOA LW flux. The skin temperature and the downward surface LW flux are also similar to those derived from the ERA-Interim reanalysis data for

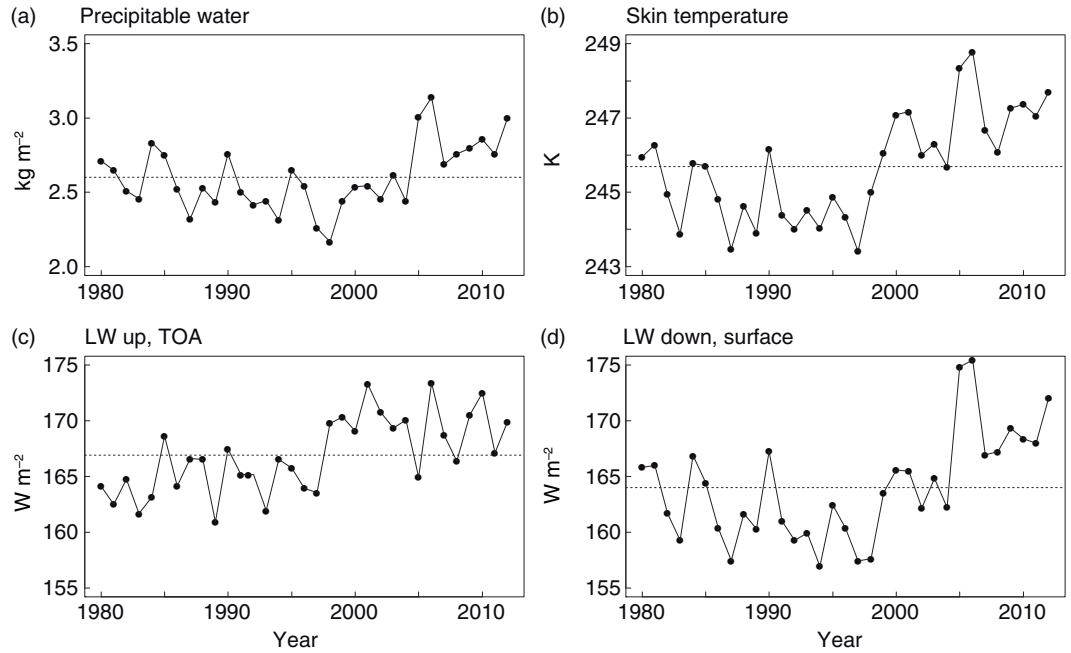

Fig. 5. Winter mean precipitable water (a), skin temperature (b), upward longwave flux at top-of-atmosphere (c) and downward longwave flux at the surface (d), averaged for the polar region north of 70°N.

Table 3. Correlation coefficients between winter average parameters[#]

Polar cap average (> 70°N)		Downward LW surface	Precipitable water	Skin temperature	Upward LW TOA[##]
Zonal section average					
400–700 hPa (~ 70°N)					
30°W–30°E	[*vort*]	0.34	0.18	0.34	0.10
	TFHV	0.33	0.23	0.27	−0.13
60°E–120°E	[*vort*]	**−0.41**	−0.26	**−0.43**	−0.12
	TFHV	**−0.73**	**−0.69**	**−0.67**	−0.17
700–1000 hPa (~ 70°N)					
30°W–30°E	[*vort*]	0.12	−0.01	0.08	−0.20
	TFHV	0.37	0.27	0.29	−0.04
60°E–120°E	[*vort*]	**−0.46**	−0.33	**−0.50**	−0.25
	TFHV	**−0.66**	**−0.60**	**−0.66**	−0.27

[#]LW = longwave flux; [*vort*] = mean positive vorticity; TFHV = time fraction of high vorticity ($vort > 10^{-5}$ s^{-1}); bold font for $p < 0.01$.
[##]TOA is top-of-atmosphere.

1990–2010 (Woods et al., 2013), whose interannual variations were found to be associated with intense moisture intrusions to the Arctic.

Table 3 shows correlation coefficients calculated for mean positive vorticity with the Arctic mean climate parameters and for TFHV with the same parameters. Significant negative correlations (at $p < 0.01$) are found between TFHV over the WCS and the downward surface LW flux ($r = -0.73$ for TFHV 400–700 hPa), precipitable water (−0.69) and skin temperature (−0.67) (compare curves in Fig. 4d and 5). The correlation between TFHV and TOA LW flux is insignificant (−0. 17). The correlation coefficients are smaller for 700–1000 hPa TFHV and for mean positive vorticity in both layers. Similar correlations are insignificant over the northern Atlantic. These correlations suggest that the cyclonic circulation (or a lack of) over the WCS may vary with and even possibly plays a role in driving winter climate in the Arctic. The causes of circulation changes over Siberia are beyond the scope of this paper.

5. Summary

In this study we calculate the ANET to the Arctic based on meteorological data from the NCEP/NCAR reanalysis for the period of 1979–2012. During this period the ANET decreased in all seasons, while the Arctic temperature increased and sea ice decreased. The downward trends are statistically significant for winter and annual mean fluxes, but not for other seasons. We calculated the energy fluxes, the mean variance of v and the mean positive local vorticity by cross-sections (400 hPa – surface, every 30° from 0° to 360°E) for each winter. Linear regressions of the time-series show a general increase of transient eddy activity and associated energy fluxes over the northern Atlantic, and a general decrease over the west and central Siberia. Inter-winter variations in transient eddy activity, as measured by the time fraction of high local vorticity, over the WCS are significantly anti-correlated with the Arctic climate.

6. Acknowledgements

Catherine Raphael drew Figure 1. Vaishali Naik, Michael Winton and Rong Zhang commented on the manuscript. Two anonymous reviewers provided constructive comments that led to significant improvements of the manuscript.

References

Alexeev, V., Esau, I., Polyakov, I., Byam, S. and Sorokina, S. 2012. Vertical structure of recent Arctic warming from observed data and reanalysis products. *Clim. Change* **111**, 215–239.

Arguez, A., Karl, T. R., Squires, M. F. and Vose, R. S. 2013. Uncertainty in annual rankings from NOAA's global temperature time series. *Geophys. Res. Lett.* **40**, 5965–5969. DOI: http://dx.doi.org/10.1002/2013GL057999

Barnes, E. A., Dunn-Sigouin, E., Masato, G. and Woolings, T. 2014. Exploring recent trends in Northern Hemisphere blocking. *Geophys. Res. Lett.* **41**, 638–644. DOI: http://dx.doi.org/10.1002/2013GL058745

Cai, M. 2005. Dynamical amplification of polar warming. *Geophys. Res. Lett.* **32**, L22710. DOI: http://dx.doi.org/10.1029/2005GL024481

Chung, C. E., Cha, H., Vihma, T., Räisänen, P. and Decremer, D. 2013. On the possibilities to use atmospheric reanalyses to evaluate the warming structure in the Arctic. *Atmos. Chem. Phys.* **13**, 11209–11219.

Chylek, P., Folland, C. K., Lesins, G., Dubey, M. K. and Wang, M.-Y. 2009. Arctic air temperature change amplification and the Atlantic multidecadal oscillation. *Geophys. Res. Lett.* **36**, L14801. DOI: http://dx.doi.org/10.1029/2009GL038777

Comiso, J. C. 2012. Large decadal decline of the Arctic multiyear ice cover. *J. Clim.* **25**, 1176–1193.

Comiso, J. C., Parkinson, C. L., Gersten, R. and Stock, L. 2008. Accelerated decline in the Arctic sea ice cover. *Geophys. Res. Lett.* **35**, L01703. DOI: http://dx.doi.org/10.1029/2007GL031972

Flanner, M. G., Zender, C. S., Randerson, J. T. and Rasch, P. J. 2007. Present-day climate forcing and response from black carbon in snow. *J. Geophys. Res.* **112**, D11202. DOI: http://dx.doi.org/10.1029/2006JD008003

Graversen, R. G. 2006. Do Changes in the midlatitude circulation have any impact on the Arctic surface air temperature trend? *J. Clim.* **19**, 5422–5438.

Graversen, R. G., Langen, P. L. and Mauritsen, T. 2014. Polar amplification in CCSM4: contributions from the lapse rate and surface albedo feedbacks. *J. Clim.* **27**, 4433–4450.

Graversen, R., Mauritsen, T., Tjernström, M., Källén, E. and Svensson, G. 2008. Vertical structure of recent Arctic warming. *Nature* **451**, 53–56.

Kalnay, E., Kanamitsu, M., Kistler, R., Collins, W., Deaven, D. and co-authors. 1996. The NCEP/NCAR 40-year reanalysis project. *Bull. Am. Meteorol. Soc.* **77**, 437–471.

Mahajan, S., Zhang, R. and Delworth, T. L. 2011. Impact of the Atlantic meridional overturning circulation (AMOC) on Arctic surface air temperature and sea ice variability. *J. Clim.* **24**, 6573–6581.

Nakamura, N. and Oort, A. H. 1988. Atmospheric heat budgets of the polar regions. *J. Geophys. Res.* **93**(D8), 9510–9524.

Peings, Y. and Magnusdottir, G. 2014. Forcing of the wintertime atmospheric circulation by the multidecadal fluctuations of the North Atlantic Ocean. *Environ. Res. Lett.* **9**, 034018, 8 pp.

Peixoto, J. P. and Oort, A. H. 1992. *Physics of Climate*. American Institute of Physics, New York, 520 pp.

Perlwitz, J., Hoerling, M. and Dole, R. 2015. Arctic tropospheric warming: causes and linkages to lower latitudes. *J. Clim.* **28**, 2154–2167.

Pithan, F. and Mauritsen, T. 2014. Arctic amplification dominated by temperature feedbacks in contemporary climate models. *Nat. Geosci.* **7**, 181–184.

Screen, J. A., Deser, C. and Simmonds, I. 2012. Local and remote controls on observed Arctic warming. *Geophys. Res. Lett.* **39**, L10709. DOI: http://dx.doi.org/10.1029/2012GL051598

Screen, J. A. and Simmonds, I. 2010. The central role of diminishing sea ice in recent Arctic temperature amplification. *Nature* **464**, 1334–1337.

Serreze, M. C., Barret, A., Stroeve, J., Kindig, D. and Holland, M. 2009. The emergence of surface-based Arctic amplification. *Cryosphere* **3**, 11–19.

Serreze, M. C. and Barry, R. G. 2005. *The Arctic Climate System*. Cambridge University Press, Cambridge, 385 pp.

Serreze, M. C. and Barry, R. G. 2011. Processes and impacts of Arctic amplification: a research synthesis. *Global Planet. Change* **77**, 85–96.

Smedsrud, L. H., Esau, I., Ingvaldsen, R. B., Eldevik, T., Haugan, P. M. and co-authors. 2013. The role of the Barents Sea in the Arctic climate system. *Rev. Geophys.* **51**, 415–449. DOI: http://dx.doi.org/10.1002/rog.20017

Sorteberg, A. and Walsh, J. E. 2008. Seasonal cyclone variability at 70°N and its impact on moisture transport into the Arctic. *Tellus* **60A**, 570–586.

Swann, A. L., Fung, I. Y., Levis, S., Bonan, G. B. and Doney, S. C. 2010. Changes in Arctic vegetation amplify high-latitude warming through the greenhouse effect. *Proc. Nat. Acad. Sci.* **107**(4), 1295–1300.

Taylor, P. C., Cai, M., Hu, A., Meehl, G. A., Washington, W. and co-authors. 2013. A decomposition of feedback contributions to polar warming amplification. *J. Clim.* **26**, 7023–7043.

Trenberth, K. E. 1991. Climate diagnostics from global analysis: conservation of mass in ECMWF analysis. *J. Clim.* **4**, 707–722.

Winton, M. 2006. Amplified Arctic climate change: what does surface albedo feedback have to do with it? *Geophys. Res. Lett.* **33**, L03701. DOI: http://dx.doi.org/10.1029/2005GL025244

Woods, C., Caballero, R. and Svensson, G. 2013. Large-scale circulation associated with moisture intrusions into the Arctic during winter. *Geophys. Res. Lett.* **40**, 1–5. DOI: http://dx.doi.org/10.1002/grl.50912